2015

High strength and ductility of ultrathin laminate foils using accumulative roll bonding and asymmetric rolling

Hailiang Yu
University of Wollongong, hailiang@uow.edu.au

A Kiet Tieu
University of Wollongong, ktieu@uow.edu.au

Syamsul Hadi
sh879@uowmail.edu.au

Cheng Lu
University of Wollongong, chenglu@uow.edu.au

Ajit R. Godbole
University of Wollongong, agodbole@uow.edu.au

See next page for additional authors

Publication Details

Yu, H., Tieu, A. Kiet., Hadi, S., Lu, C., Godbole, A. & Kong, C. (2015). High strength and ductility of ultrathin laminate foils using accumulative roll bonding and asymmetric rolling. Metallurgical and Materials Transactions A: Physical Metallurgy and Materials Science, 46 (2), 869-879.

High strength and ductility of ultrathin laminate foils using accumulative roll bonding and asymmetric rolling

Abstract
As product miniaturization is becoming widely popular, many microparts are being produced by microforming of sheets/foils, whose strength needs to be able to maintain structural stability of the micro-components. In addition, their strength and ductility of foils generally reduce with a reduction in the thickness due to the size effect. In this paper, we report the fabrication of an aluminum laminate foil using a combined process of accumulative roll bonding (ARB) and asymmetric rolling (AR). It was found that this improves both strength and ductility. TEM results show that the laminate structures produced by ARB develop an inhomogeneous microstructure with nanoscale grains and abnormal coarsening in some grains during AR processing. Both these effects result in an improved ductility and strength. Using these rolled products, micro-cups of very small wall thickness/cup diameter ratio (1/200) have been successfully fabricated by micro-deep drawing without the need for annealing.

Keywords
Aluminum alloy; Nanostructure; Abnormal grain growth; Rolling; Deep drawing; Ultrathin laminate foil

Disciplines
Engineering | Science and Technology Studies

Publication Details
Yu, H., Tieu, A. Kiet., Hadi, S., Lu, C., Godbole, A. & Kong, C. (2015). High strength and ductility of ultrathin laminate foils using accumulative roll bonding and asymmetric rolling. Metallurgical and Materials Transactions A: Physical Metallurgy and Materials Science, 46 (2), 869-879.

Authors
Hailiang Yu, A Kiet Tieu, Syamsul Hadi, Cheng Lu, Ajit R. Godbole, and Charlie Kong

High Strength and Ductility of Ultrathin Laminate Foils Using Accumulative Roll Bonding and Asymmetric Rolling

HAILIANG YU[a,b*], KIET TIEU[a], SYAMSUL HADI[a,d], CHENG LU[a], AJIT GODBOLE[a], CHARLIE KONG[c]

[a] *School of Mechanical, Materials & Mechatronics Engineering, University of Wollongong, NSW 2500, Australia.*

[b] *School of Mechanical Engineering, Shenyang University, Shenyang 110044, China.*

[c] *Electron Microscope Unit, University of New South Wales, Sydney, NSW 2052, Australia.*

[d] *Mechanical Engineering Department, State Polytechnic of Malang, P.O. Box 04 Malang 65100, East Java, Indonesia*

Abstract: As product miniaturization is becoming widely popular, many microparts are being produced by microforming of sheets/foils, whose strength needs to be able to maintain structural stability of the micro components. In addition, their strength and ductility of foils generally reduces with a reduction in the thickness due to the size effect. In this paper, we report the fabrication of an aluminum laminate foil using a combined process of Accumulative Roll Bonding (ARB) and Asymmetric Rolling (AR). It was found that this improves both strength and ductility. TEM results show that the laminate structures produced by ARB develop an inhomogeneous microstructure with nanoscale grains and abnormal coarsening in some grains during AR processing. Both these effects result in an improved ductility and strength. Using these rolled products, micro-cups of very small wall thickness/cup diameter ratio (1/200) have been successfully fabricated by micro deep drawing without the need for annealing.

***Keywords*:** Aluminum alloy; Nanostructure; Abnormal grain growth; Rolling; Deep drawing; Ultrathin laminate foil

* Corresponding author: YU H.L., hailiang@uow.edu.au or yuhailiang1980@tom.com

I. INTRODUCTION

Product miniaturization is a trend for facilitating product usage, enabling product functions to be implemented in microscale geometries, and aimed at reducing product weight, volume and cost.[1] A number of microchannels and microcups have been produced by sheets/foils microforming.[2, 3] The smaller the microparts, the thinner the foils need to be. These foils should be strong enough to maintain the structural stability of the microparts. In addition, the size effects on the behavior of microformed materials have assumed an increasing importance.[4-6] For rolled monolayer foils, the size effect is often evident in drawn cups. Recently, Fu and Chan[7] carried out a review of microforming technologies, and they noted that the fracture strain decreased with a reduction in the workpiece size in tensile tests on sheet metal. It was observed that fracture results from localised shear in individual grains. Thin cold-rolled and annealed copper foils of varying thicknesses with a scaled geometry and comparable microstructure were tested in tension by Simons *et al.*[8] They found that when the foil thickness was reduced from 250 μm to 10 μm, the fracture strain decreased from approximately 0.2 to 0.002 for cold-rolled foils and from 0.35 to 0.15 for annealed foils respectively. To study the size effects on fracture, Fu and Chan[9] conducted tensile tests on annealed pure copper foils with varying thicknesses and grain sizes. It was found that the flow stress, fracture stress/strain and the number of microvoids on the fracture surface decreased with decreasing specimen size/grain size ratio. Nanostructured/ ultrafine-grained sheets/foils fabricated using Severe Plastic Deformation (SPD) techniques can be used to offset size effects on

workpieces during microforming and to improve the structural stability of microparts. Ma *et al.*[10] used an SPD technique, called equal channel angular pressing, to fabricate ultrafine-grained copper sheets which were subsequently manufactured in a micro deep drawing process. They found that the ultrafine-grained copper has potential applications in microforming. These considerations suggest that it would be interesting and significant to produce nanostructured sheets/foils with special properties.

Special properties such as high strength and ductility of nanostructured materials have attracted widespread attention from researchers.[11-13] Variants of the SPD techniques such as asymmetric cryorolling,[14, 15] Accumulative Roll Bonding (ARB)[16, 17] and Asymmetric Rolling (AR)[18, 19] have been developed to enable bulk fabrication of nanostructured/ultrafine-grained metal sheets/foils. The ARB and AR techniques can be used to produce continuous products and are more feasible for practical application in industries. The ARB technique was developed by Tsuji *et al.*[16] and has been used successfully to produce nanostructured/ultrafine-grained specimens[16, 17]. In the AR process, sheets/foils are passed between rolls that either have different diameters or rotate at different angular speeds. AR is also considered a potential technology for production of nanostructured/ultrafine-grained materials. It is possible to obtain a quasi-uniform shear strain distribution through the thickness of the material under certain rolling conditions. AR-processed Al sheets[19] and bimetallic foils[18] show an excellent ductility during tensile tests. In addition, the AR technique can produce thinner foils. AR is different from conventional rolling as

regards parameters such as rolling load, shear strain, and minimum permissible thickness[20]. AR has a significant potential for a variety of industrial applications because it requires lower rolling pressure while simultaneously improving the product shape. The influence of the roll speed ratio on reduction in unit pressure on the rolls was studied by Kawalek *et al*.[20] They found that the magnitude of the total rolling force could be reduced by 27% by AR.

Generally, ductility and strength are conflicting properties in nanostructured bulk metals.[21] In addition, with ever-thinner foils, the size effect results in reduced ductility and higher strength.[22] In the present study, we combined the ARB and AR techniques to produce aluminum laminate foils composed of 416 layers. TEM results show that the laminate structures by ARB changes into inhomogeneous microstructure with nanoscale grains and some abnormal coarse grains during AR. This results in improved foil ductility and strength. The ARB- and AR-processed foils were successfully used to produce micro-cups without fracture.

II. EXPERIMENTAL PROCEDURE

Aluminum AA1235 sheets with 300 μm thickness were used. The main chemical composition (mass %) of the material used was Al=99.35, Fe=0.42, Si=0.10, Ti=0.02, Zn=0.012, Ni=0.003, Mn=0.002, Cu=0.001, and others.

The ARB experiments were carried out on a Hille-100 rolling mill. The AR experiments were carried out on the ARB-processed sheets on a multifunction rolling mill. The rolling speed ratio between the upper and lower rolls was set as 1.3, which results in the best bonding during laminate AR.[23] **Fig. 1** shows a schematic

illustration of the process. In Step 1, 13 layers (each 300 μm thickness) were stacked and were rolled to 390 μm in one pass. In Step 2, the rolled multilayer laminates were cut into two halves, surface treated, stacked, and rolled with a reduction ratio of around 56% at a temperature of 473 K[24] in order to achieve a good bonding quality. After five ARB cycles, foils made up of 416 (13×2^5) layers were produced, and the final foil thickness was 205 μm. In Step 3, the ARB-processed sheets were subjected to two AR passes at room temperature. The thickness of foil was 85 μm and 45 μm after the first and second AR passes respectively.

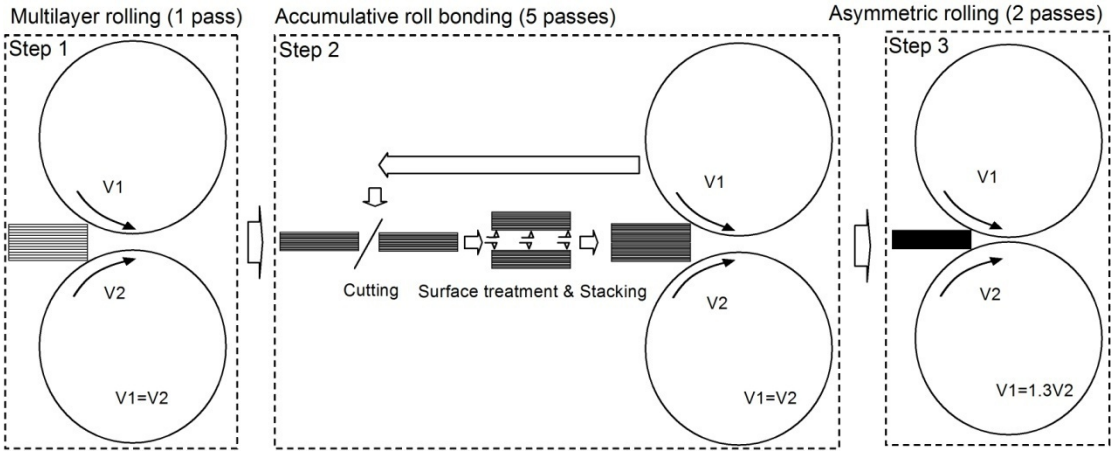

Fig. 1− Illustration of the processing schedule for nanostructural foils.

Tensile tests with a strain rate of 1.0×10^{-3} s^{-1} were carried out on the foil samples using an INSTRON machine. The tensile tests were carried out three times for each thickness. Subsequently, an FEI xT Nova Nanolab 200 Dualbeam workstation was used to prepare thin foil specimens from the rolled samples for TEM observation. A Philips CM200 Field Emission Gun Transmission Electron Microscope (FEG/TEM) equipped with a Bruker Energy Dispersive X-ray (EDAX) Spectroscopy system operating at an accelerating voltage of 200 kV was used to investigate the details of the microstructure. The Digital Micrograph software was used to determine the grain

size in the TEM images. The morphology of the fractured surface of samples was studied with a Zeiss Auriga Field Emission Scanning Electron Microscope (FESEM) operating at 20 kV, with a working distance of about 15 mm. Finally, rolled foils having a thickness of 45 μm were used to produce micro-cups of diameter 8.26 mm with a blank diameter of 14 mm.

III. RESULTS

The engineering stress vs. engineering strain curves during tensile testing of the annealed and ARB- and AR-processed foils are shown in **Fig. 2**. The engineering fracture strain of the annealed sheets is 0.064. After the fifth ARB pass, it reduces slightly to 0.055. After the first AR pass, the engineering fracture strain reduces to 0.048. However, after the second AR pass, the engineering fracture strain increases to 0.057. In the present experiments, we found no reduction in engineering fracture strain although the foil thickness was reduced by 85%. In addition, we found that the tensile strength increases significantly, as seen in **Fig. 2**. After the fifth ARB pass, the tensile stress is 133 MPa. After the second AR pass, the tensile stress increases into 147 MPa, an increase of 10.5% over the ARB-processed samples.

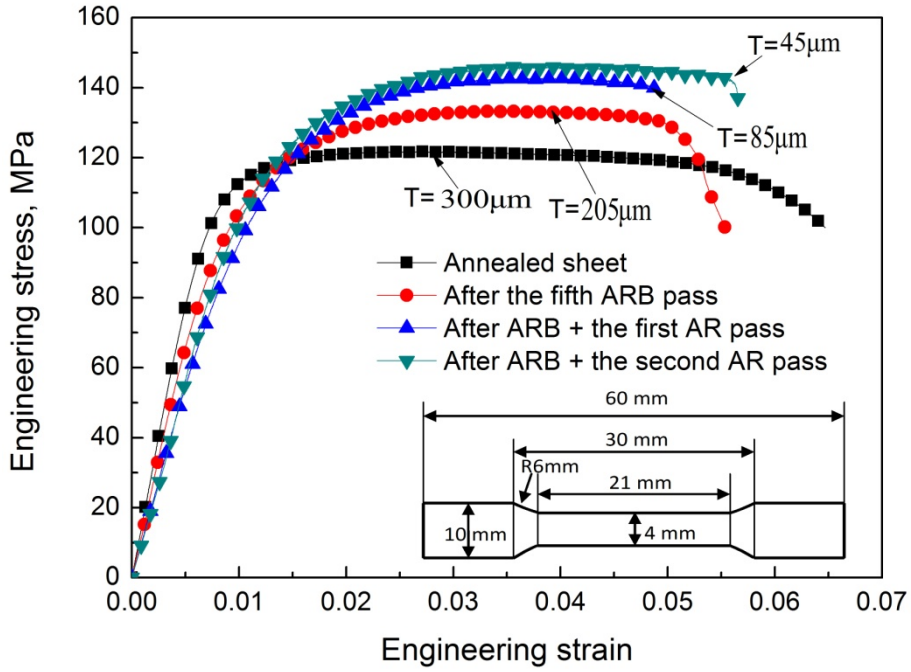

Fig.2− Engineering stress vs engineering strain curves of laminate sheets/foils.

Figures 3a to **3f** show the progressive change in the sample microstructures. In Fig. 3a, the original sheet is seen to be composed of coarse grains, which undergo refinement during the rolling process. With an increase in the number of rolling passes, the grain size gradually decreases. In ARB processing, the grains were refined to laminate structures, as shown in **Fig. 3c**. After the first AR pass, some of laminate grains were seen to coarsen and while other grains were further refined. With subsequent rolling passes, the rolled laminate structure grains change into refined equiaxed grains, as shown in **Fig. 3f**.

Figures 4a to 4e show the progressive change in grain size distribution of the samples. **Fig. 4f** shows the mean and the maximum grain size after each pass. After the second ARB pass, the mean grain size is 731 nm, the maximum grain size is 1150 nm, and most of grains range from 600 nm to 900 nm in size, as shown in Fig. 4a. In Fig. 4b, the grains are seen to be further refined. The mean grain size is reduced to

507 nm, and the maximum grain size is also reduced to 846 nm. In addition, the majority of grains range from 400 nm to 700 nm in size. After the fifth ARB pass, the mean grain size is reduced slightly to 486 nm, while the maximum grain size is still around 850 nm. Fig. 4c shows that most of grains range from 300 nm to 600 nm in size. However, in the AR process, the maximum grain sizes and the mean grain size change in two contrary directions. As shown in Fig. 4d, the maximum grain size grows to 989 nm, and the mean grain size continues to decrease to 462 nm. Grains ranging from 300 nm to 400 nm in size are obvious more than others. After the second AR pass, there are more coarse grains and the maximum grain size reaches 1126 nm, but the mean grain size decreases further to 441 nm. The majority of grains range from 200 nm to 600 nm in size. It is obvious that this change in grain size during AR improves both the strength and the ductility of the foils. As seen in Fig. 4f, the mean grain size decreases continuously, and the reduction after the fifth ARB pass is small. In addition, the maximum grain size decreases continuously in the ARB process, and increases in the AR process.

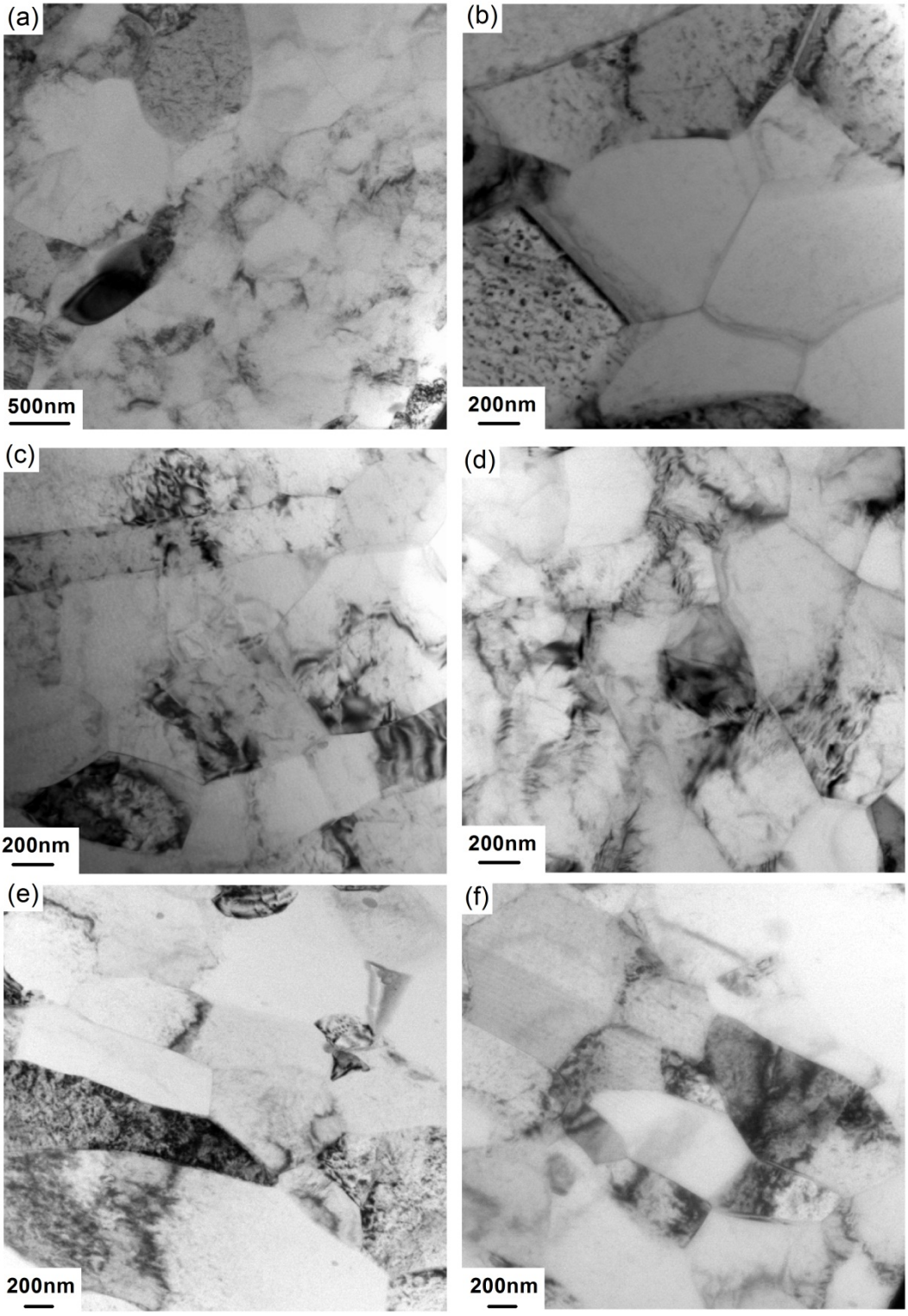

Fig. 3− TEM images of samples. (a) initial sheet, (b) after the second ARB pass, (c) after the third ARB pass, (d) after the fifth ARB pass, (e) after the first AR pass, and (f) after the second AR pass.

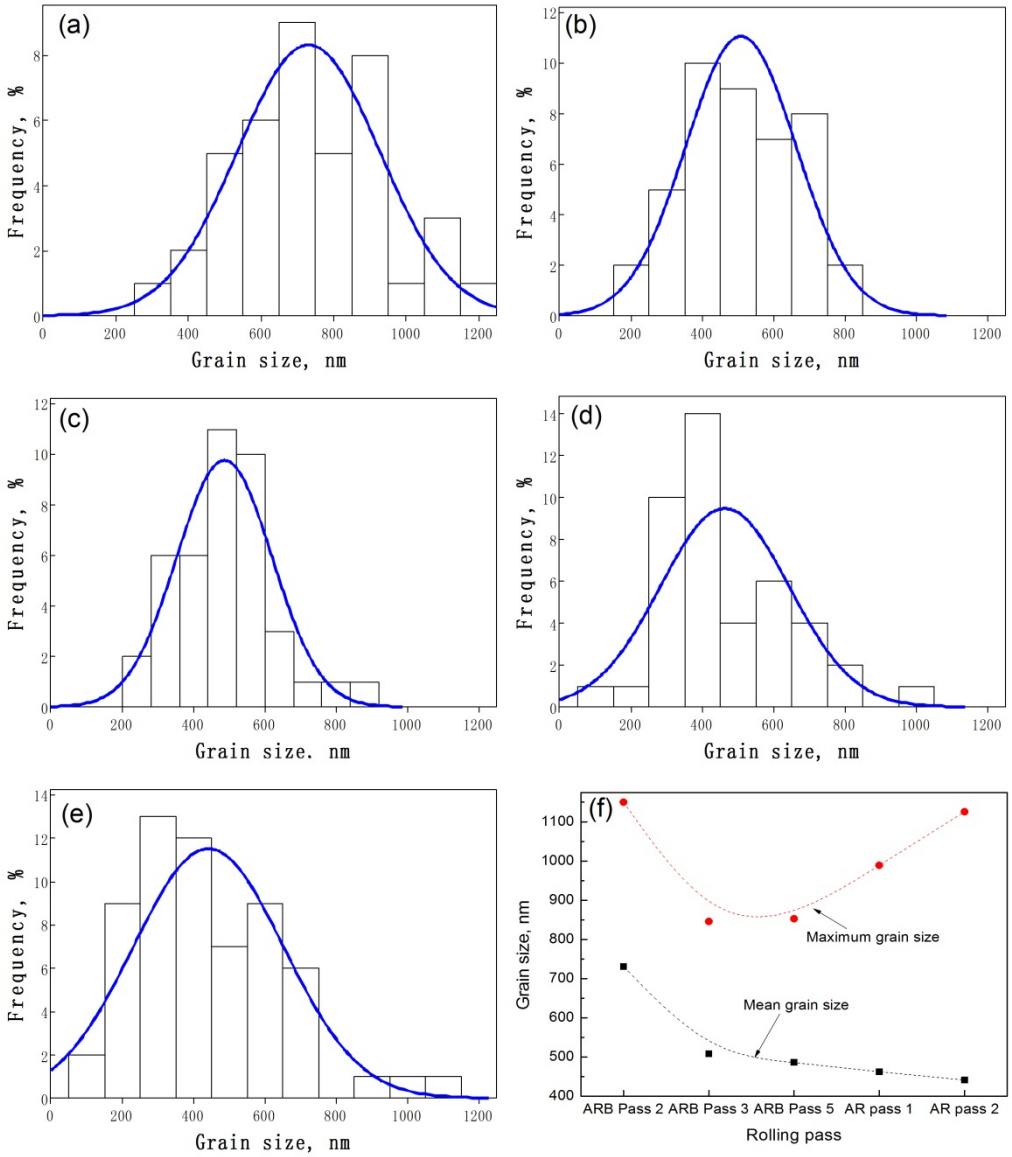

Fig. 4− Grain size distribution after the second ARB pass (a), the third ARB pass (b), the fifth ARB pass (c), the first AR pass (d), the second AR pass (e) and the mean and the maximum grain size after different rolling passes (f).

Fig. 5 shows the images of typical fracture profiles for the annealed, ARB- and AR-processed samples after a tensile test. Before rolling process, the fracture angle of test sample is 69º. With the ARB and AR passes, the fracture angles of samples gradually decreases. After the fifth ARB pass, the fracture angle of sample reduces to 63º, which becomes 60º after the second AR pass. This fracture angle value is similar to the observation in Refs. [25, 26], which is a typical fracture angle value for the

nanostructured foils such as Al, Cu and Ni-Fe after tensile test.

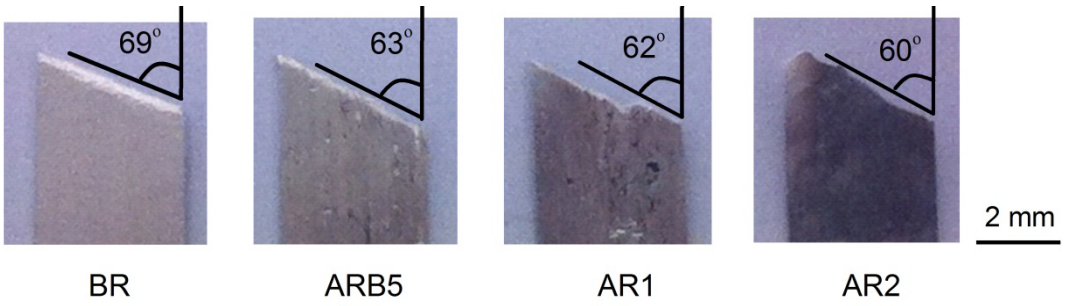

Fig. 5–Image of typical fracture profiles for samples Before Rolling (BR), after the fifth ARB pass (ARB5), the first AR pass (AR1) and the second AR pass (AR2).

Fig. 6 shows SEM images of the fracture surfaces of the samples after a tensile test. The annealed aluminium sample shows a high ductility, and there are large and deep dimples on the fracture surface, as shown in **Fig. 6a**. However, the ductility of the samples after the fifth ARB pass reduces greatly,[16] in which the dimples are smooth and shallow, as shown in **Fig. 6b**. As seen in **Fig. 6c and Fig. 6d**, after the AR processing, the density of the dimples on the fracture surface increases compared with that after the fifth ARB pass**.** This indicates an improvement in the ductility during the AR process.

For nanostructured foils, it has been suggested that the area reduction ratio is a good measure of their ductility.[25] From volume conservation, the final cross-sectional area (A_{final}) can be converted into a true fracture strain, as shown in Eq. (1)[25],

$$\varepsilon_{axial} = \ln(A_{initial} / A_{final}) = \ln(\frac{1}{1-q}) \quad (1)$$

where $A_{initial}$ is the cross-section area before the tensile test, q is the area reduction ratio. As shown in **Fig. 6**, the thicknesses after necking are 40.8 μm, 146.2 μm, 42.4 μm and 9.9 μm for the samples before rolling, after the fifth ARB pass, the first AR

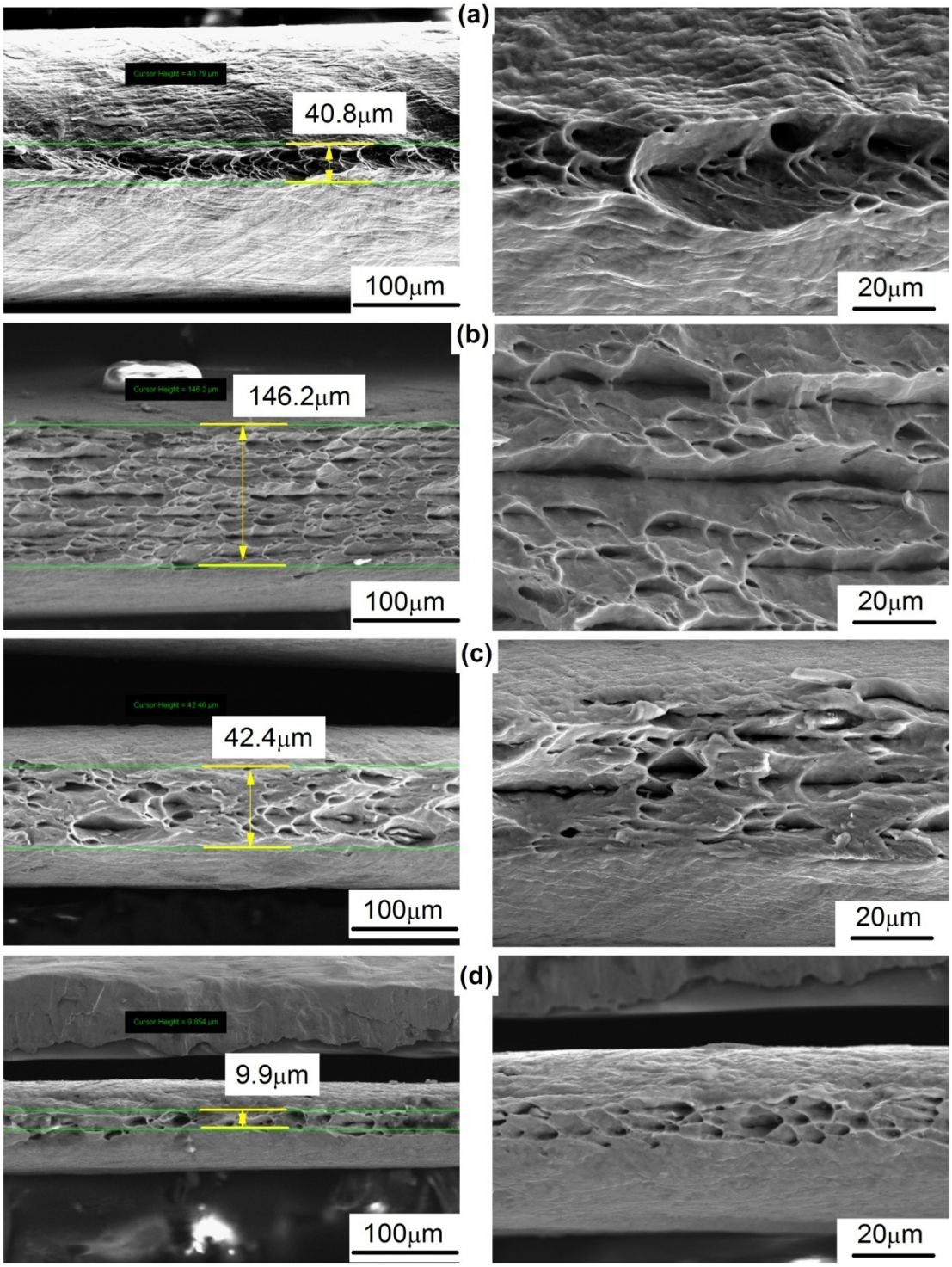

Fig. 6–SEM images of fracture surfaces (a) before rolling, (b) after fifth ARB pass, (c)after the first AR pass and (d) after the second AR pass.

pass and the second AR pass respectively. The true fracture strains for the samples were calculated using Eq. (1). **Fig. 7** shows the area reduction ratio and true fracture

strain at different stages in the process. For the annealed foils, the true fracture strain reaches 2.0. After five passes of ARB processing, the true fracture strain of foils reduces to 0.4. In general, for nanostructured materials, the ductility reduces as the strength increases. However, in this experiment, the true fracture strain of the foils improves with strength for the samples after AR processing. After the first AR pass, the true fracture strain increases to 0.7, which then increases further to 1.5 after the second AR pass.

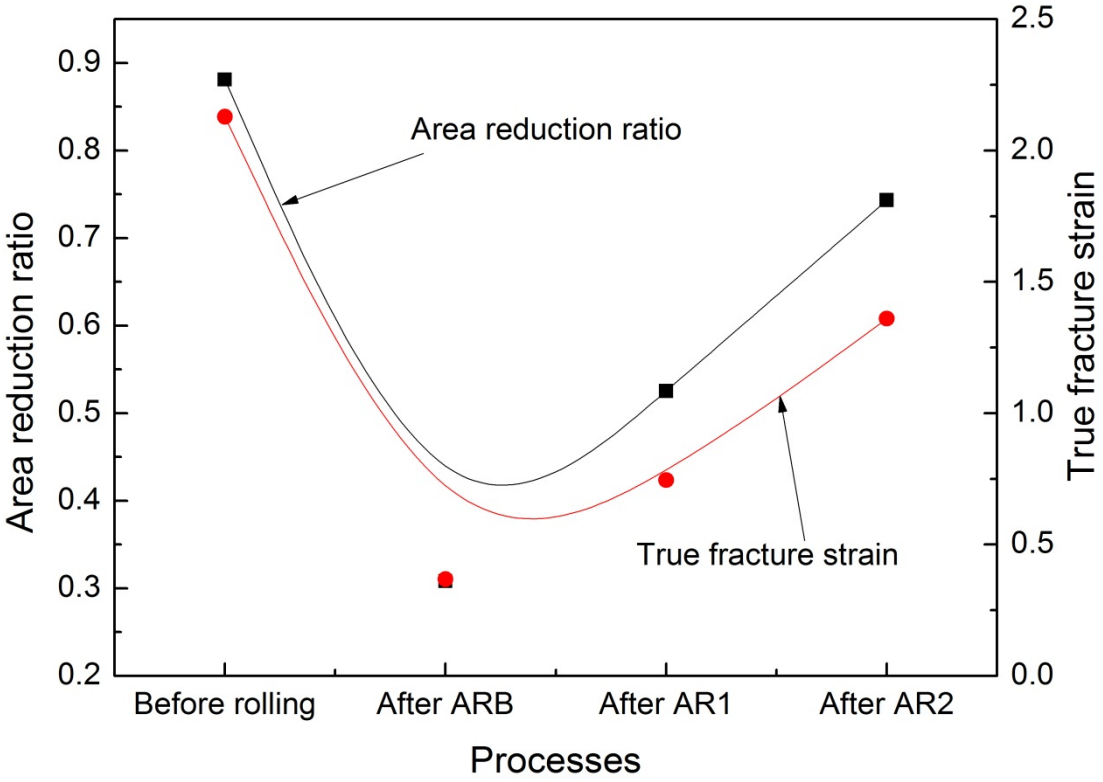

Fig. 7- Area reduction ratio and true fracture strain of samples.

These findings in **Fig. 2** and **Fig. 7** suggest that AR could significantly improve both the ductility and the strength of aluminum laminate foils. In order to test their improved properties, the foils after the second AR pass were subjected to a micro-deep drawing process without annealing to produce micro-cups. The

micro-cups are shown in **Fig. 8**. In these 8.26 mm diameter cups, the wall thickness is less than 45 μm, which is only 1/200 of the cup diameter. There are no fractures seen on the cup walls, implying that the laminate foils have a high ductility. Some wrinkles were observed due to high compressive stress on the thin wall.

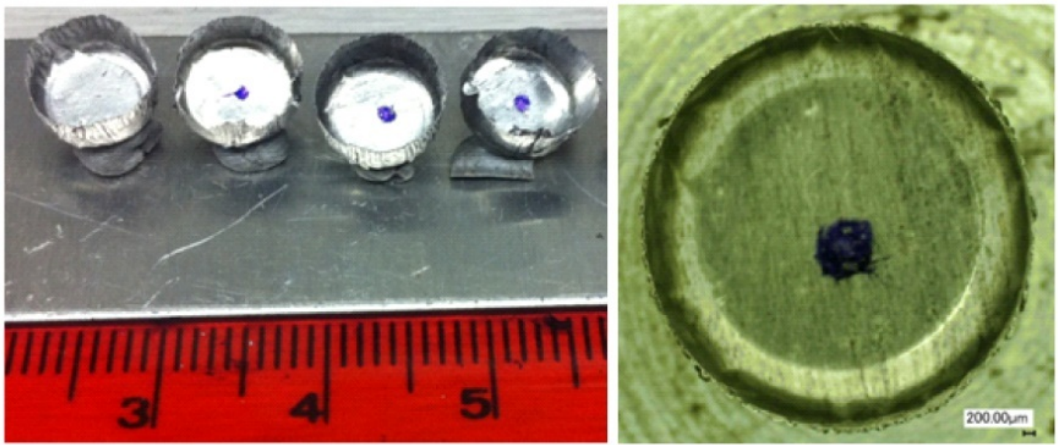

Fig. 8− Micro-cups without fracture with nanostructured laminate foils of thickness 45 μm after the second AR pass without annealing.

IV. DISCUSSION

A. *Strength and ductility improvement of nanostructured laminate foils*

As shown in **Fig. 2**, the yield strength of foils improves as a result of ARB and AR. It is easy to understand the improvement in yield strength of the foils in terms of the Hall-Petch relationship:

$$\sigma_y = \sigma_0 + k_y / \sqrt{D} \tag{2}$$

where σ_y is the yield stress after deformation, σ_0 the yield stress after annealing, k_y the Petch parameter, and D the mean grain size. As seen in **Fig. 4f**, the yield stress of the foil increases with a reduction in the mean grain size.

The improvement in both strength and toughness is a vital requirement for most

structural materials. However, for some nanostructured metals, ductility and strength are generally conflicting properties. As described by Ritchie,[21] as the quest continues for stronger and harder materials, bulk structural materials without an appropriate fracture resistance have little to no use. Thus, for nanostructured metals, it is important to improve their ductility, which generally could be improved by the following methods: (1) *Reducing stacking fault energy and increasing solute content*: Huang *et al.*[27] analyzed the effect of stacking fault energy on the equilibrium grain size and tensile properties of nanostructured copper and copper-aluminum alloys. They reported that with increasing solute content and decreasing stacking fault energy not only the strength but also the ductility of nanostructured copper alloys increased substantially. Yu *et al.*[15] analyzed the improvement in ductility by ageing in AA6061 samples. Due to a high density of nanosized precipitates formed during ageing, a higher number of dislocations are accumulated, which results in enhanced ductility. Lu *et al.*[28] carried out cold rolling experiments on bulk nanocrystalline pure copper. They pointed out that the super-plastic deformation of nanocrystalline copper originates from a deformation mechanism dominated by grain boundary activity rather than lattice dislocation. (2) *Application of nanotwins*: Shen *et al.*[29] tested the tensile properties of an electro-deposited Cu sample with a high density of nano-scale growth twins. They found that both the strength and the ductility increase with a decrease in thickness of the twin lamellae. Wei *et al.*[30] reported a way of enhancing the strength of twinning-induced plasticity steel with no ductility trade-off. (3) *Controlling the grain size distribution*: Fang *et al.*[31] reported experiments on a

nano-grained copper film confined by a coarse-grained copper substrate with a gradient in grain-size transition. The sample exhibited a ten-fold increase in the yield strength and a tensile plasticity comparable to that of the coarse-grained substrate. The samples could sustain a tensile true strain exceeding 100% without cracking. Wang *et al.*[32] reported a mechanism for developing an inhomogeneous microstructure in nanostructured copper where strain hardening mechanisms can stabilize the tensile deformation, and lead to a high tensile ductility.

In the current study, we found an inhomogeneous microstructure combined with nanosize grains and abnormal coarse grains in AR-processed samples. This is similar to the observation reported in Ref. [32]. As shown in Fig. 4d and 4f, the majority of grains reduce in size with a higher rolling deformation, but some grains are seen to coarsen abnormally. As shown in **Fig. 3b** and **Fig. 3c**, in the ARB process, the grains were refined to nanosized laminated structures. In the AR process, some laminate grains grow abnormally to become coarse grains, while most of the remaining grains are further refined, as shown in **Fig. 3f**. In **Fig. 4f**, both the mean grain size and thickness of foil after the first AR pass are reduced compared with that after the fifth ARB pass, but the ductility of the foil increases slightly (In **Fig. 7**) due to the appearance of coarse grains during the first AR pass as shown in **Fig. 4d**. It is seen in **Fig. 4e** that after the second AR pass, the frequency of coarse grains increases. This, in turn, greatly increases the foil ductility.

B. *Abnormal grain growth mechanism during AR*

It is easy to understand why an increase in strain brings about grain refinement. The

relationship between dislocation density and strain is shown in Eq. (3):[33]

$$\rho_g = (bl)^{-1}\varepsilon \tag{3}$$

where ρ_g is the total generated dislocation density, b the Burgers vector, l the mean free path for dislocation movement, and ε the strain. However, as shown in Fig. 4f, some grains are seen to grow abnormally during AR.

Generally, if the temperature of sample is higher than a certain threshold value, the grains will grow in size. At high temperature, materials show both normal continuous grain growth and abnormal discontinuous grain growth. During an abnormal grain growth, the difference in individual grain size increases due to some of the grains growing rapidly.[34] Hillert[34] believed that the abnormal grain growth could develop in a material annealed at high temperature under three conditions: (i) normal grain growth cannot take place due to the presence of second-phase particles, (ii) the average grain size is less than a certain value, (iii) there is at least one grain much larger than the average. It is obvious that none of the above three conditions can explain the abnormal grain growth seen in **Fig. 3f**. During AR, the temperature rise of the foils increases with increasing roll speed ratio. But, when the reduction is about 40%, the temperature rise of the foils is generally less than 373 K.[35] Yu *et al.*[36] analyzed the recovery mechanisms in nanostructred aluminium when the temperature is less than 373 K. The laminate boundaries are generally flat, with the curvature maximum at triple junctions. The boundary velocity v is usually assumed to be proportional to the driving pressure P, with the mobility M as the proportionality factor (v=PM). If the migration is thermally activated and the driving pressure is given

as a function of the boundary curvature ($P=2\gamma/r$), the boundary velocity will be:

$$v = \frac{2\gamma}{r} M_0 \exp(-\frac{Q_b}{RT}) \tag{4}$$

where γ is the boundary energy, r the radius of curvature, M_0 a pre-exponential constant, and Q_b the activation energy for boundary migration. It was found that for pure aluminium during grain growth,[36] M_0 = 0.125 $m^4J^{-1}s^{-1}$, Q_b = 130 $kJmol^{-1}$, and γ = 0.324 Jm^{-2} for a high angle boundary. Therefore, when the temperature of the foils rises to 373 K for radius of curvature r = 50 nm, the velocity will be 3.5×10^{-12} ms^{-1}. Because the rolling process lasts only for a few seconds, the temperature rise during AR causing the grain boundary migration can be neglected.

Besides the grain growth driven by temperature, shear stress also could drive the grain boundary migration and result in grain growth. Haslam *et al.*[37] proposed two grain growth mechanisms during the deformation: (1) growth due to curvature-driven grain boundary migration and (2) growth resulting from grain rotation-induced coalescence. Generally, the AR process leads to a higher shear stress compared with the conventional rolling process. **Fig. 9** shows the shear stress distribution in the roll deformation zone compared with conventional rolling and AR by finite element simulation. It is obvious that the AR produces higher shear stress.

It is widely acknowledged that shear stresses can induce dislocation motion. The motion of low-angle grain boundaries, which consist of dislocation arrays, under shear stress can be described by the collective movement of the individual dislocations in these boundaries.[38] In addition, shear stress promotes texture evolution during grain growth, and grain growth can serve as a stress relief

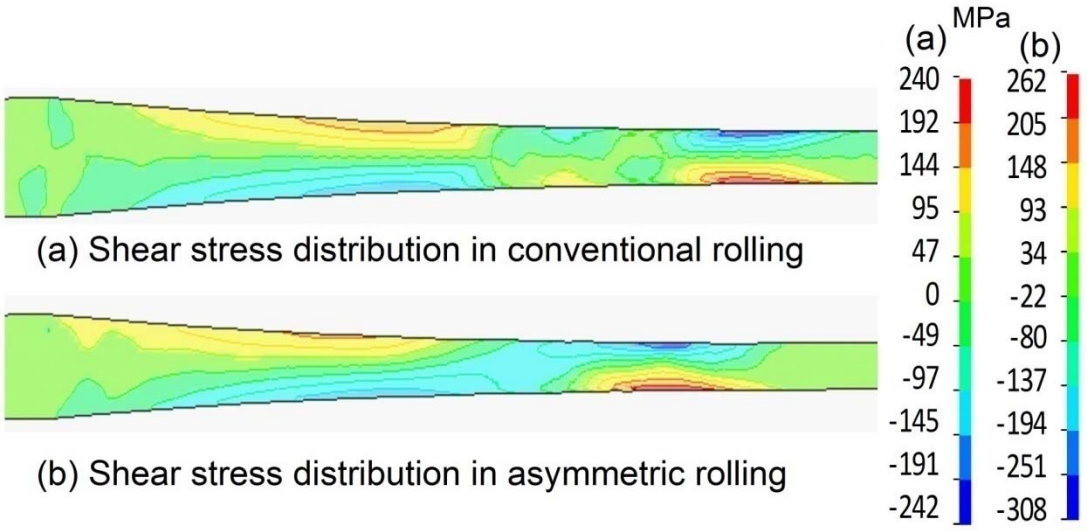

Fig. 9− Shear stress distribution when the foil is rolled from 205 μm to 85 μm (with the same reduction ratio in first AR pass) by (a) conventional rolling and (b) AR.

mechanism in both elastically isotropic and anisotropic materials, and can also promote plastic yielding. Rollett *et al.*[39] believed that the abnormal grain growth can occur by two distinct mechanisms. Both of these mechanisms are related to anisotropy in the properties of the grain boundaries: anisotropic grain boundary energy and mobility. Shear stress applied to a grain boundary can induce its normal motion. Stress-induced grain boundary migration can cause grain shape change and grain rotation, leading to plastic deformation of polycrystalline materials without diffusion or slip in the grains. Washburn and Parker[40] investigated planar low-angle grain boundaries in Zn under the influence of an external shear stress and observed the continuous motion with polarized light in an optical microscope. Shan *et al.*[41] reported in situ dynamic TEM observations of nanocrystalline nickel films with an average grain size of about 10 nm, which show that the grain boundary-mediated process is a prominent deformation mode. According to traditional conception, a

mechanical stress does not couple with a high-angle boundary. Winning *et al.*[42] pointed out that at high temperatures the response of high-angle grain boundaries to shear changes from coupling to sliding until the coupling disappears. In 2005, mechanical grain growth was observed by Zhang *et al.*[43] in nanocrystalline Cu under an indenter at liquid nitrogen temperature. They found the grains grew from 20 nm to 400 nm at cryogenic temperature after 30 minutes. Li *et al.*[44] pointed out that the material must be pure enough so that free dislocations are available to move out of the boundary. But the boundary should not be in the lowest-energy state so that extra dislocations are available to be emitted by stress. For ARB-processed sheets, there should be some oxygen atoms at the interface between layers. Tang *et al.*[45] found that the oxygen atoms pin the boundaries, preventing stress-assisted grain growth. In addition, for ARB-processed pure aluminum laminates, most of grains are high-angle grains, and there are some solute elements in the matrix. Thus the grain growth caused by stress-driven grain boundaries migration is also difficult at low temperature (less than 373 K).

In 2002, Moldovan *et al.*[46] proposed a grain growth mechanism: grain rotation leading to coalescence of neighboring grains via elimination of the common grain boundary between them. They assumed that the grain boundary energy depends on the misorientation angle between any two neighboring grains, and the change of the orientation of one grain due to rotation leads to a change in the misorientations of all the grain boundaries surrounding the grain change. When two neighboring grains assume the same orientation, they coalesce forming a single larger grain. Wang *et al.*

[47] used nanobeam electron diffraction and a series of dark field images technique to investigate the deformation mechanism of nanocrystalline Ni in response to in situ tensile deformation under TEM. They validated the deformation-induced grain rotation and growth mechanism. **Fig. 10** shows an abnormally coarse grain resulting from AR processing in a detail of **Fig. 3f**. In the figure, the merging of four grains into a coarse grain can be seen. From the analysis above, in this growth mechanism, it is likely that four grains grow into a coarse grain due to stress-induced grain rotation during AR.

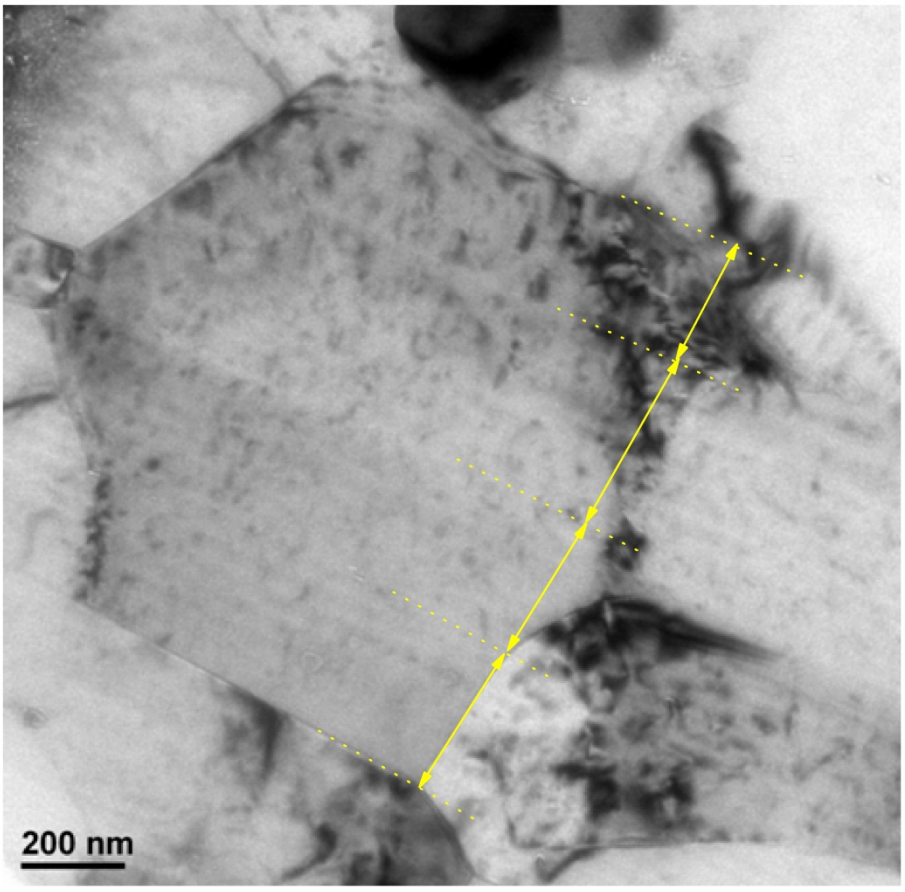

Fig. 10− Abnormal grain growth by four grains in foil during AR.

C. *Thickness size effect in nanostructured laminate foils*

For metallic sheets and foils, thickness size effects are significant.[22] Suh *et al.*[48] found that the tensile strength and ductility of Al 6K21-T4 sheets decreased almost linearly with a reduction in thickness, when the thickness was less than a critical value. With a reduction in the sheet thickness, the grains on the free surface are less constrained and can be deformed more easily at a substantially lower flow stress than is the case in the bulk state. As shown in **Fig. 11a**,[48] for annealed Al 6K21-T4 sheets of grain size 40 μm, as the thickness of the sheet is reduced from 1600 μm to 400 μm, the engineering fracture strain is reduced from 0.25 to 0.15 and the tensile stress also decreases slightly. A similar phenomenon was also observed by Simons *et al.*[8] who carried out tensile tests on thin rolled & annealed copper foils of different thicknesses. As shown in **Fig. 11b**, when the thickness is reduced from 250 μm to 10 μm, the fracture strain decreases from 0.35 to 0.15 for annealed samples with grain size 15 μm. However, as shown in **Fig. 11c**, the strength of the foils increases greatly after ARB & AR. The engineering fracture strain of the foils also increases slightly, although the thickness of foils decreases significantly in the present study. The thickness of the annealed sheets is 300 μm, and the thickness of the foils after the second AR pass is reduced to 45 μm. In addition, as shown in **Fig. 7**, the true fracture strain of the ARB-processed foils increases from 0.4 to 1.5 after two AR passes. At this point, the tensile stress increases by 21% and the ductility of the foils is much greater than that with thickness 205 μm after the ARB process.

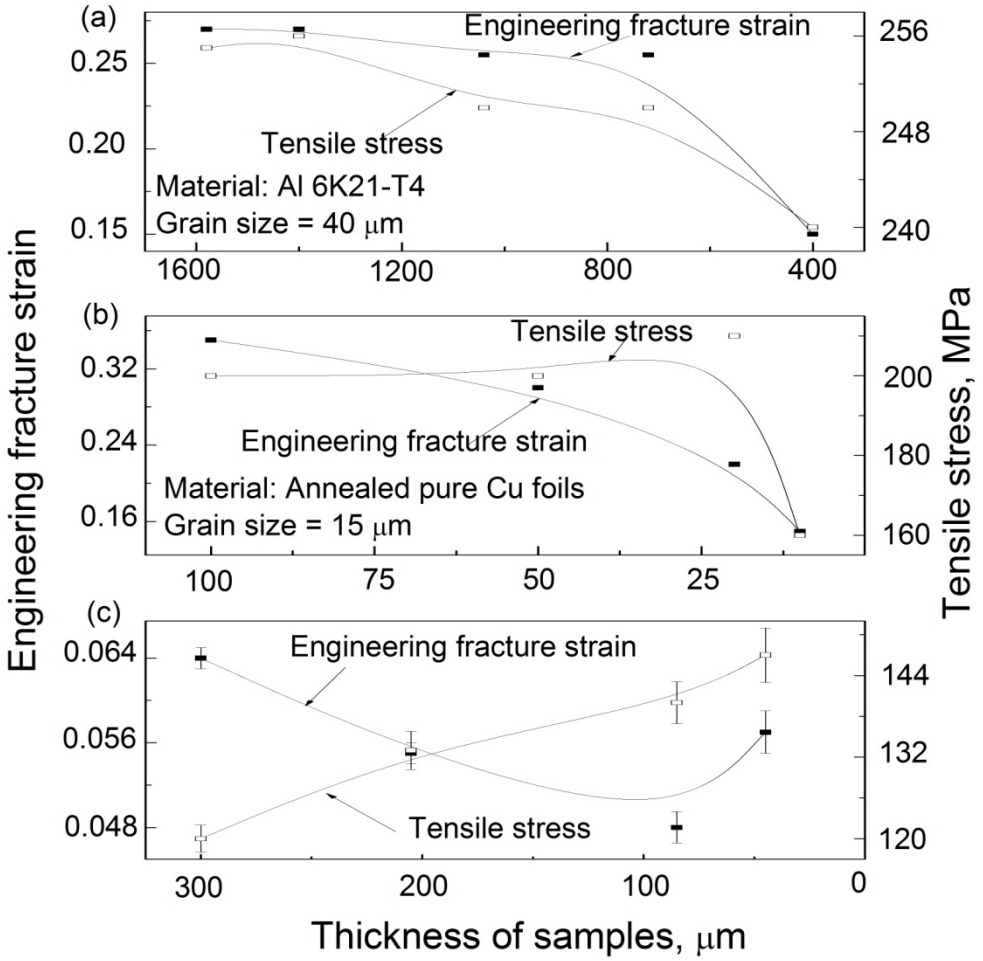

Fig.11− Thickness size effect during tensile process, (a) for Al 6K21-T4 with coarse grains,[48] (b) for annealed pure Cu foils,[8] and (c) for the samples in current experiments.

For metal sheets and foils with coarse grains, with a reduction in the sample thickness, the grains on the free surface are less constrained and more easily deformed at a substantially lower flow stress than is the case in the bulk state. Kals *et al.*[49] expressed the volume fraction α of grains having a free surface, as shown in Eq. (5):

$$\alpha = 1 - \frac{(w-2d)(t-2d)}{wt} \tag{5}$$

where w is the specimen width, t the specimen thickness, and d the average grain size. When the specimen width is much larger than the grain size ($w>>d$), Eq. (5) can be

simplified to:

$$\alpha = \frac{2d}{t} \tag{6}$$

Generally, as the thickness decreases, the relative surface area per volume of a specimen increases. In the experiments by Suh *et al.*, α is 0.5% when the thickness is 1600 μm, increasing to 20% when the thickness is 400 μm. Simons *et al.* showed that α is 30% when the thickness is 100 μm, increasing to 300% when the thickness is 10 μm. In these two cases, the thickness size effect is obvious. In the present experiments, α is 0.4% when the thickness is 205 μm after ARB processing, and 1.9% when the thickness is 45 μm after the second AR pass. It is seen that the thickness size effect is only slight for the nanostructured aluminium laminate foils.

V. CONCLUSIONS

In summary, 45 μm thick laminate foils of 416 layers were produced using a combination of the accumulative roll bonding and asymmetric rolling techniques. Compared with the coarse-grained metal foils, these foils exhibited reduced size (thickness) effect during microforming. Using these foils, we successfully produced micro-cups with wall thickness 45 μm by micro-deep drawing without fracture and without the necessity of annealing.

The AR process improved both the ductility and strength of the ARB-processed sheets/foils. In the AR process, most of the laminated structured grains were further refined. But some of the laminated structured grains were found to coarsen

abnormally, resulting in an inhomogeneous microstructure. The inhomogeneous microstructure leads to both higher strength and greater ductility.

During AR, the high shear stress leads to abnormal grain growth. There are two grain growth mechanisms during the deformation: growth due to curvature-driven grain boundaries migration and growth resulting from grain rotation-induced coalescence. In the current study, it is probable that the shear stress-induced grain rotation resulted in the abnormal grain growth.

ACKNOWLEDGMENTS

The lead author gratefully acknowledges the financial support from the Vice-Chancellor's Fellowship Grant and URC small grant at the University of Wollongong, and from the National Natural Science Foundation of China through Grant 51105071. SH gratefully to Directorate General for Higher Education (DIKTI) of the Republic of Indonesia for supporting the PhD scholarship.

REFERENCES

[1] Y.P. Chen, W.B. Lee and E. Nakamachi: *Acta. Mech. Solida Sin.*, 2010, vol.23, pp.36-48.

[2] W.L. Chan, and M.W. Fu: *Mater. Sci. Eng. A*, 2012, vol. 556, pp. 60-67.

[3] I. Irthiea, G. Green, S. Hashim, and A. Kriama: *Int. J. Mach. Tool. Manuf.*, 2014, vol.76, pp. 21-33.

[4] A. Molotnikov, R. Lapovok, C.F. Gu, C.H.J. Davies and Y. Estrin: *Mater. Sci. Eng. A.*, 2012, vol.550, pp.312-319.

[5] M.D. Uchic, D.M. Dimiduk, J.N. Florando and W.D. Nix: *Science*, 2004, vol.305, pp.986-989.

[6] P.A. Dubos, E. Hug, S. Thibault, M. Ben Bettaieb and C. Keller: *Metall. Mater. Trans. A*, 2013, vol.44A, pp.5478-5487.

[7] M.W. Fu and W.L. Chan: *Int. J. Adv. Manuf. Technol*., 2013, vol.67, pp.2411-2437.

[8] G. Simons, C. Weippert, J. Dual and J. Villain: *Mater. Sci. Eng. A*, 2006, vol.416, pp.290-299.

[9] M.W. Fu and W.L. Chan: *Mater. Des.*, 2011, vol.32, pp.4738-4746.

[10] X. Ma, R. Lapovok, C. Gu, A. Molotnikov, Y. Estrin, E.V. Pereloma, C.H.J. Davies and P.D. Hodgson: *J. Mater. Sci*., 2009, vol.44, pp.3807-3812.

[11] R. Valiev: *Nature Mater*., 2013, vol.12, pp.289-291.

[12] Y.T. Zhu and X.Z. Liao: *Nature Mater.*, 2004, vol.3, pp.351-352.

[13] G. Liu, G.J. Zhang, F. Jiang, X.D. Ding, Y.J. Sun, J. Sun and E. Ma: *Nature Mater.*, 2013, vol.12, pp.344-350.

[14] H.L. Yu, C. Lu, K. Tieu, X.H. Liu, A. Godbole and C. Kong: *Sci. Rep.*, 2012, vol.2, art. no.772.

[15] H.L. Yu, K. Tieu, C. Lu, X.H. Liu, A. Godbole and C. Kong: *Mater. Sci. Eng. A*, 2013, vol.568, pp.212-218.

[16] N. Tsuji, Y. Ito, Y. Saito and Y. Minamino: *Scripta Mater*., 2002, vol.47, pp.893-899.

[17] H.L. Yu, C. Lu, K. Tieu and C. Kong: *Mater. Manuf. Processes*, 2014, vol.29, pp.448.

[18] H.L. Yu, C. Lu, K. Tieu, A. Godbole, L.H. Su, Y. Sun, M. Liu, D.L. Tang and C. Kong: *Sci. Rep.*, 2013, vol.3, art. no.2373.

[19] H.K. Kim, H.W. Kim, J.H. Cho and J.C. Lee: *Mater. Sci. Eng. A*, 2013, vol.574, pp.31-36.

[20] A. Kawalek, H. Dyja, S. Mroz and M. Knapinski: *Metalurgija*, 2011, vol.50, pp.163-166.

[21] R.O. Ritchie: *Nature Mater.*, 2011, vol.11, pp.817-822.

[22] X.X. Huang: *Acta Metall. Sin.*, 2014, vol.50, pp.137-140.

[23] H.L. Yu, K. Tieu, C. Lu and A. Godbole: *Metall. Mater. Trans. A*, 2014, vol. 45, pp. 4038-4045.

[24] M.Z. Quadir, O. Al-Buhamad, L. Bassman and M. Ferry: *Acta Mater*., 2007, vol.55, pp.5438-5448.

[25] J.A. Sharon, H.A.Padilla and B.L. Boyce: *J. Mater. Res.*, 2013, vol. 28, pp. 1539-1552.

[26] H.L. Yu, K. Tieu, C. Lu, Y.S. Lou, X.H. Liu, A. Godbole and C. Kong: *Int. J. Damage Mech.*, 2014, DOI: 10.1177/105678951438083.

[27] C.X. Huang, W. Hu, G. Yang, Z.F. Zhang, S.D. Wu, Q.Y. Wang and G. Gottstein: *Mater. Sci. Eng. A*, 2012, vol.556, pp.638-647.

[28] L. Lu, M.L. Sui and K. Lu: *Science*, 2000, vol.287, pp.1463-1466.

[29] Y.F. Shen, L. Lu, Q.H. Lu, Z.H. Jin and K. Lu: *Scripta Mater*., 2005, vol.52, pp.989-994.

[30] Y. Wei, Y. Li, L. Zhu, Y. Liu, X. Lei, G. Wang, Y. Wu, Z. Mi, J. Liu, H. Wang and

H. Gao: *Nat. Commun*., 2014, vol.5, art. no.3580.

[31] T.H. Fang, W.L. Li, N.R. Tao and K. Lu: *Science*, 2011, vol.331:1587-1590.

[32] Y. Wang, M. Chen, F. Zhou and E. Ma: *Nature*, 2002, vol.419, pp.912-915.

[33] X.G. Qiao, N. Gao and M.J. Starink: *Phil. Mag.*, 2012, vol.92, pp.446-470.

[34] M. Hillert: *Acta Metall.*, 1965, vol.13, pp.227-238.

[35] R.B. Megantoro Loorentz and Y.G. Ko: *J. Alloy. Comp.*, 2014, vol.586, pp.s254-s257.

[36] T.B. Yu, N. Hansen and X.X. Huang: *Phil. Mag.*, 2012, vol.92, pp.4056-4074.

[37] A.J. Haslam, D. Moldovan, V. Yamakov, D. Wolf, S.R. Phillpot and H. Gleiter: *Acta Mater.*, 2003, vol.51, pp.2097-2112.

[38] T.J. Rupert, D.S. Gianola, Y. Gan and K.J. Hemker: *Science*, 2009, vol.326, pp.1686-1690.

[39] A.D. Rollett, D.J. Spolovitz and M.P. Anderson: *Acta Metall.*, 1989, vol.37, pp.1227-1240.

[40] J. Washburn and E.R. Parker: *J. Metals*, 1952, vol.4, pp.1076-1078.

[41] Z. Shan, E.A. Stach, J.M.K. Wiezorek, J.A. Knapp, D.M. Follstaedt and S.X. Mao: *Science*, 2004, vol.305, pp.655-657.

[42] M. Winning, G. Gottstein and L.S. Shvindlerman: *Acta Mater.*, 2001, vol.49, pp.211-219.

[43] K. Zhang, J.R. Weertman and J.A. Eastman: *Appl. Phys. Lett*., 2005, vol.87, art. no.061921.

[44] J.C.M. Li: *Phys. Rev. Lett.*, 2006, vol.96, art. no.215506.

[45] F. Tang, D.S. Gianola, M.P. Moody, K.J. Hemker and J.M. Cairney: *Acta Mater.*, 2012, vol.60, pp.1038-1047.

[46] D. Moldovan, V. Yamakov, D. Wolf and S.R. Phillpot: *Phys. Rev. Lett.*, 2002, vol.89, art. no.206101.

[47] Y.B. Wang, B.Q. Li, M.L. Sui and S.X. Mao: Appl. Phys. Lett., 2008, vol.92, art. no.011903.

[48] C.H. Suh, Y. C. Jung and Y. S. Kim: *J. Mech. Sci. Technol.*, 2010, vol.24, pp.2091-2098.

[49] R. Kals, F. Vollertsen and M. Geiger: *Proc. Fourth Int. Conf. Sheet Metal*, Vol II, Enschede, 1996, pp.65-75.